Supporting Information - Carbon Surface Crowding and Subsurface Traffic Jam as Drivers for Methane Oxidation Activity and Selectivity on Palladium Surfaces

Ulrike Küst,[*,†,‡] Rosemary Jones,[†] Julia Prumbs,[†,‡] Alessandro Namar,[§] Mattia Scardamaglia,[¶] Andrey Shavorskiy,[¶] and Jan Knudsen[*,†,¶,‡]

†*Division of Synchrotron Radiation Research, Lund University, Box 118, SE-221 00 Lund, Sweden*

‡*NanoLund, Lund University, Box 118, SE-221 00 Lund, Sweden*

¶*MAX IV Laboratory, Lund University, Box 118, SE-221 00 Lund, Sweden*

§*Physics Department, University of Trieste, via A. Valerio 2, Trieste 34127, Italy*

E-mail: ulrike.kust@sljus.lu.se; jan.knudsen@sljus.lu.se

Solid-gas interface branch

For these measurements a cylindrical sample was mounted on a transferrable 304L stainless steel sample plate. An PID controlled IR laser was used to heat the crystal and the temperature was monitored with a type K thermocouple spot welded to the side of the crystals to ensure a precise temperature measurement. The reading was done once every third second. Before the experiments the crystal was cleaned by 1 kV Ar^+ sputtering at 1×10^{-5} mbar pressure and 10 mA emission current for 20 min followed by annealing to 650 °C. The cleanliness of the surface was confirmed by XPS survey scans. The footprint of the beam on the sample is 60 µm × 25 µm and the measured gas phase signal originates from a volume consisting of this footprint size and a height of 90 µm. The HIPP-3 electron analyzer with a 0.8 mm slit was operated in fixed acquisition mode using a 8 Hz acquisition frequency. A pass energy of 100 eV was used for the surface spectra, while 200 eV was used during gas

phase measurements such that the entire binding energy range (approximately 10% of the pass energy) could be covered by the electron analyzer in fixed acquisition mode.

Oxygen (5.0 N) and CH_4 (3.5 N) were used for the experiments. Commercial Pall gas cleaners (GLP2OXPVMM4 for O_2 and GLPSIPVMM4 for CH_4) were used on both gas lines. The gases were dosed with mass flow controllers (Brooks GF125). The stated flow values in sccm units refers to standard conditions of 20 °C and 14.696 psia (1 bar). The pressures stated in the paper were measured at the cell outlet with a Baratron capacitance gauge. The gas composition in the cell is followed by a Quadropole Mass Spectrometer which probes the gas composition in the first differential pumping stage of the electron analyzer, i.e. at a roughly 700 µm distance from the catalyst surface.

Sample preparation

To prepare the sample, a Pd(100) single crystal (6 mm diameter) was put through several oxidation and reduction cycles that roughened the surface, and, while changing color a few times (light grey, blue, green, black), the surface eventually turned polycrystalline. Survey spectra were collected throughout the measurement to check for possible contaminations. Impurities were not found at any point.

Depth profiling

The probing depths are estimated from the photoelectron kinetic energy and the universal curve for the electron mean free path in matter to be 0.6 nm for the highest surface sensitivity and 1.5 nm for the more bulk sensitive measurement. This corresponds to the probing of approximately 3 and 8 atomic layers in a Pd(100) crystal, respectively.

Scaling of mass spectrometry and APXPS gas phase data

Assuming that the sensitivity of the mass spectrometer (MS) is similar for all gas components, the measured intensities are scaled to the total pressure. Additionally, a constant background has been subtracted from the H_2 signal (c.f. Fig. S5) since we do not expect hydrogen formation in the presence of molecular oxygen and instead assume H_2O decomposition in the spectrometer. To estimate the partial pressures of the gas phase components measured in APXPS, a scaling factor was first applied to the curve-fitted intensities to account for the different photoionization cross sections of the O 1s and C 1s peaks. By dividing by the number of corresponding atoms in the probed molecule and scaling to the total pressure, partial pressures of all components were obtained.

Data analysis

All data analysis was performed in Igor Pro 8 using purpose-written scripts. Every spectrum was corrected for the analyzer transmission function and the binding energy axes were calibrated using the Fermi edge. Since the electron analyzer is more accurate at lower electron kinetic energies, the spectra measured at higher photon energies were aligned with those measured at lower photon energies by using the gas phase binding energies. Time alignment

was done using the gas phase work function shift. Polynomial background subtraction was carried out for each spectrum by fitting a polynomial to the datapoints where no components were visible. To determine the datapoint range for fitting the background subtraction the sum spectrum of all time resolved data was used (to ensure that the background subtraction did not remove any weak components). After background subtraction and normalization for varying electron transmission through the gas phase, all spectra were Fourier transformed and then the first 50 harmonics were inverse Fourier transformed. The IFT image was then curve fitted with symmetric Voigt functions with as little free parameters as possible. For example, a common Lorentzian width was used for all components (0.1 eV[1]).

Component widths and surface BEs were determined at the example of one spectrum in the entire image and then kept constant for the curve fit of the time evolution. The binding energy that was used for fitting surface carbon was 284.5 eV while SSR carbon was positioned at 284.9 eV. Surface oxygen was fitted with a binding energy of 529.7 eV. The Pd $3p_{\frac{3}{2}}$ BE was allowed to vary as well as those of the gas phase components which can be found in Fig. S5.

Fourier analysis

In short, this analysis methodology (discussed in detail in refs[2,3]) uses Fourier transformation to selectively analyze the part of the XPS signal that oscillates with the same frequency as the temperature modulation (17 mHz, c.f. Fig. 1 (M)) or multiples thereof as well as the static part. By discarding all other frequency components and by inverse Fourier transforming one can greatly improve the signal-to-noise ratio as Fig. 1 (E-H) demonstrates. For this dataset, Fourier analysis even provides better results than event averaging (c.f. ref.[4] for more details on the method) especially for the noisy O 1s data (c.f. Panel (A)) as no lock-in signal needs to be found in the image.

Time-resolved selectivity calculation

The number of moles N for each species j can be written as

$$N_j = N_{j,0} + \sum \nu_{ij} \chi_i \tag{S1}$$

where $N_{j,0}$ is the initial number of moles of species j, ν_{ij} the stochiometric coefficient of species j in reaction i, and χ_i the extent of reaction i. Since our species are measured in a flow reactor, $N_{j,0} = 0$ and we can write

$$N_j = \sum \nu_{ij} \chi_i \tag{S2}$$

which can then be used to formulate equations for each species. Thus, we obtain

$$N_{CO2} = 1 \cdot \chi_{II} + 1 \cdot \chi_I \tag{S3}$$
$$N_{CO} = 1 \cdot \chi_{III} \tag{S4}$$
$$N_{H2} = 2 \cdot \chi_V \tag{S5}$$
$$N_{H2O} = 2 \cdot \chi_{II} + 2 \cdot \chi_{III} + 2 \cdot \chi_{IV} \tag{S6}$$
$$N_C = 1 \cdot \chi_V + \chi_{IV} \tag{S7}$$

where the roman numerals refer to the reaction equations in Fig. 4 (E). Hence, we directly get

$$\chi_{III} = N_{CO} \qquad \text{and} \tag{S8}$$
$$\chi_V = 0.5 \cdot N_{H2}. \tag{S9}$$

We can assume that the pathways (I) and (IV) cannot coexist since their sum would be pathway (II) again. Thus, if pathway (IV) is present, we set $\chi_I = 0$ which leads to

$$\chi_{II} = N_{CO2} \qquad \text{and} \tag{S10}$$
$$\chi_{IV} = 0.5 \cdot N_{H2O} - N_{CO} - N_{CO2}. \tag{S11}$$

Likewise, if pathway (I) is present, then $\chi_{IV} = 0$ and we obtain

$$\chi_{II} = 0.5 \cdot N_{H2O} - N_{CO} \qquad \textit{and} \tag{S12}$$
$$\chi_I = N_{CO2} - \chi_{II} \tag{S13}$$
$$= N_{CO2} - 0.5 \cdot N_{H2O} - N_{CO} \tag{S14}$$

which defines all desired reaction extents.

Error discussion

Possible sources of error during the measurement include such that are made due to the principle of measurement and such that result from the data analysis. An example of the first category is that the resolution of the beamline decreases for increasing photon energies. Even if this effect is small, it might have lead to the overlooking of small peaks that are only present deeper in the bulk.

Most of the errors made result from the data analysis, however. The most significant one is probably the direct comparison of MS and XPS data. Not only are the resulting signals measured at different locations in the chamber (XPS very localized at the sample surface, MS averaged over the whole chamber in the analyzer cone), they might also have different sensitivities to different gases that we did not calibrate for. Due to the fact that the MS averages over the whole chamber and is located a bit away from the sample, the gas signals measured in the spectrometer cannot experience sharp changes but are rather smoothed out. This can, for example lead to the over- or underestimation of carbon deposition effects using the hydrogen signal.

An error that results solely from XPS is due to the depth profiling technique. Since the measured photoelectrons from deeper layers decay exponentially within the material, a direct comparison of surface and bulk component intensities most likely leads to a significant underestimate of the amount of probed bulk atoms.

In the beginning of the analysis of the XPS raw data, an error is introduced to the intensity of the components due to the chosen normalization for changing gas attenuation and beam intensity fluctuations.

During the FT analysis of the XPS raw data, an additional error is introduced to the curve shape (see detailed discussion in ref[3]) and probably the component intensity. The magnitude of this error is, however, difficult to estimate.

The subsequent curve fit to the IFT image leads to error bars in the intensity evolution of the individual components resulting from the accuracy of the curve fit.

Supporting Figures

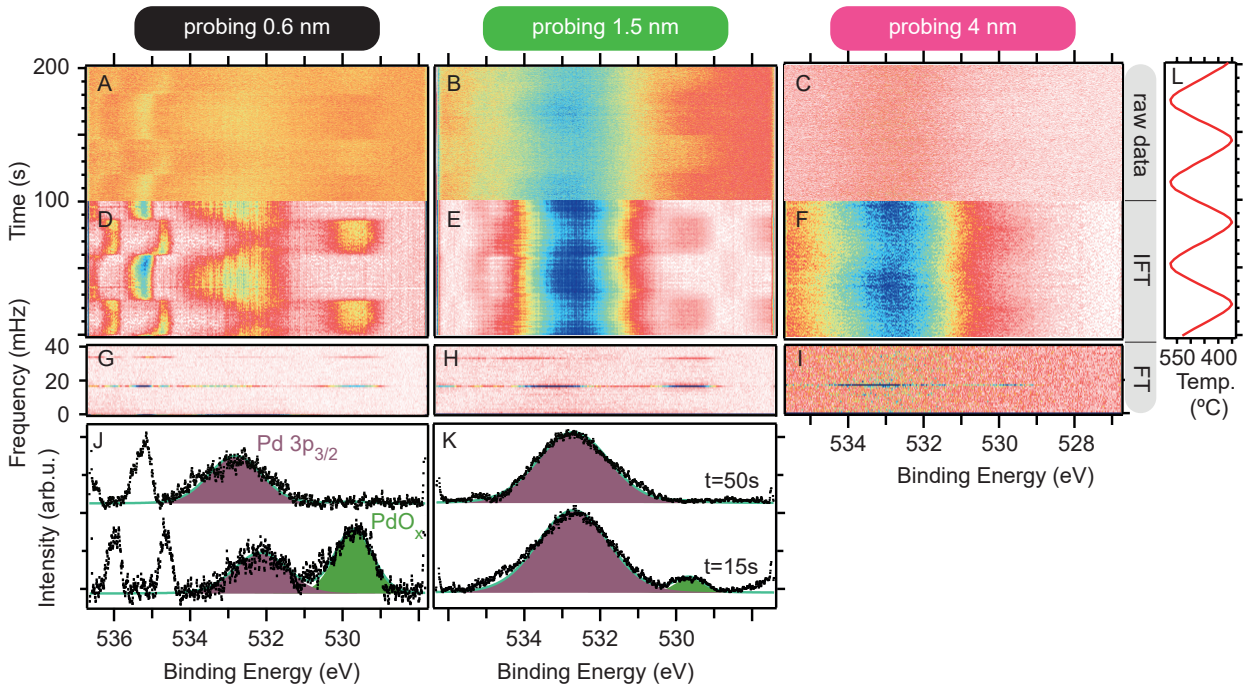

Figure S1: Measured O 1s raw data (A,B,C), inverse Fourier transform of 50 harmonics (D,E,F) including the 0 Hz component of the Fourier transform as shown in (G,H,I), and examples of the curve fit to the IFT at two times (J,K) are shown together with the temperature modulation (L).

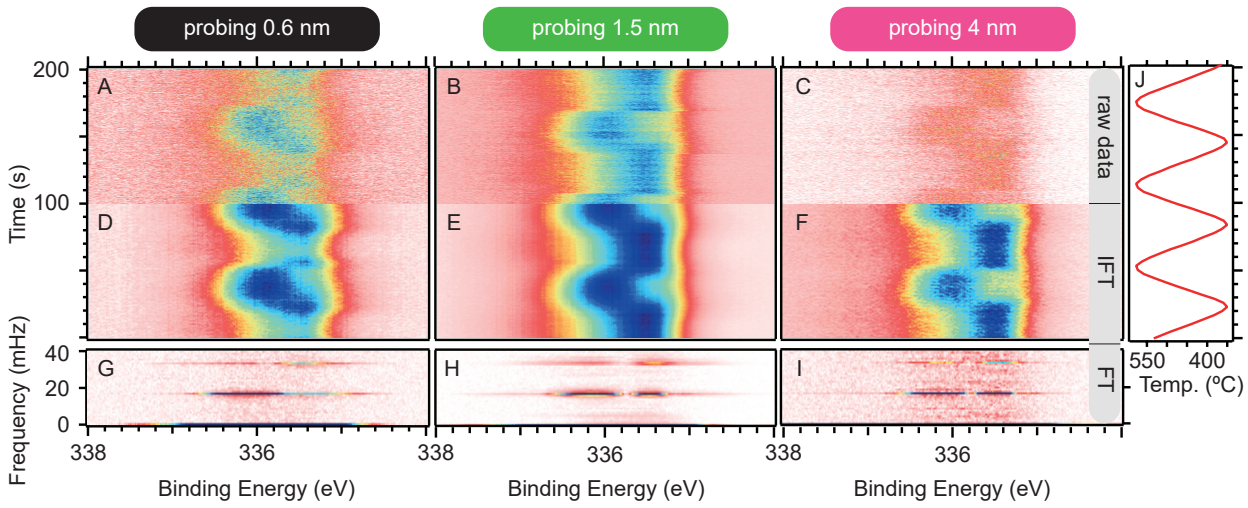

Figure S2: Measured Pd 3d raw data (A,B,C), inverse Fourier transform of 50 harmonics (D,E,F) including the 0 Hz component of the Fourier transform as shown in (G,H,I), and the temperature modulation (J) are shown.

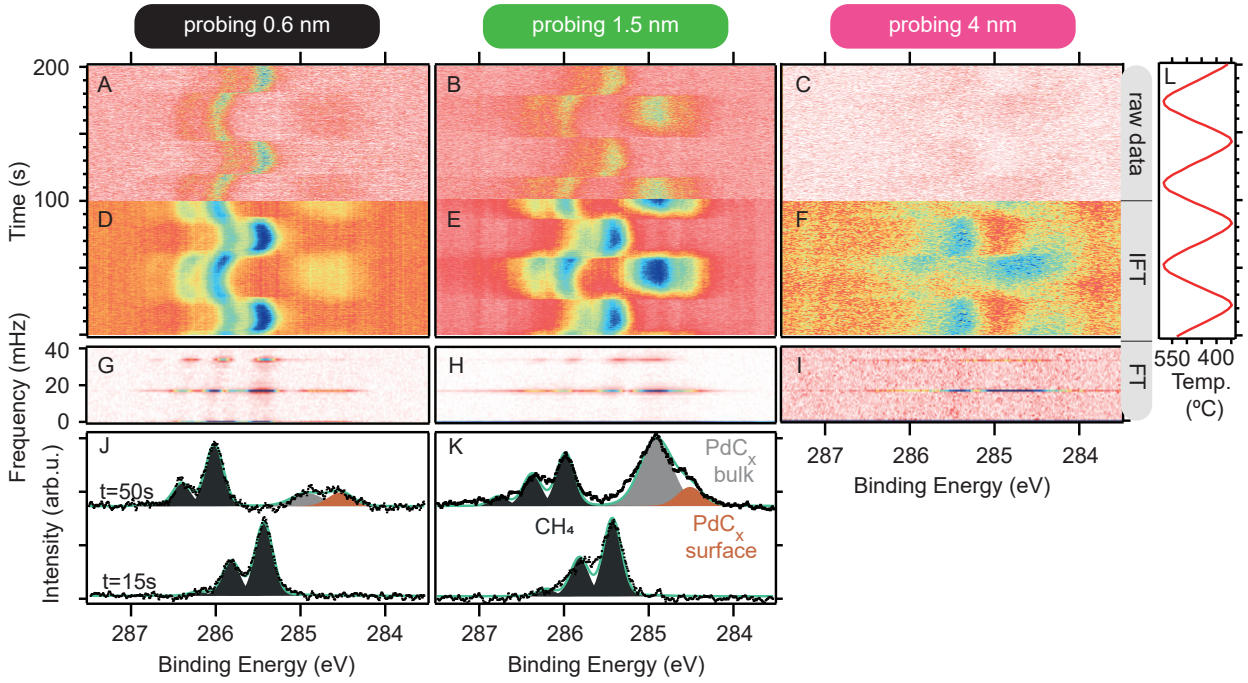

Figure S3: Measured C 1s raw data (A,B,C), inverse Fourier transform of 50 harmonics (D,E,F) including the 0 Hz component of the Fourier transform as shown in (G,H,I), and examples of the curve fit to the IFT at two times (J,K) are shown together with the temperature modulation (L).

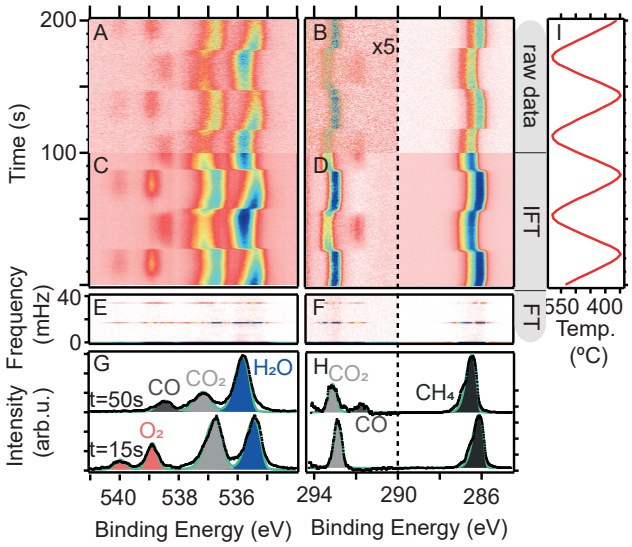

Figure S4: Measured raw data for the O 1s (A) and C 1s (B) gas phase spectra. The respective inverse Fourier transforms (IFT) of 50 harmonics are shown in (C) and (D) based on the Fourier transforms in (E,F). Panel (I) shows the temperature modulation signal applied to the catalyst. Examples of the curve fitting are shown at $t = 15\,\mathrm{s}$ and $t = 50\,\mathrm{s}$. The high BE side of the C 1s spectra has been magnified 5 times for better visibility.

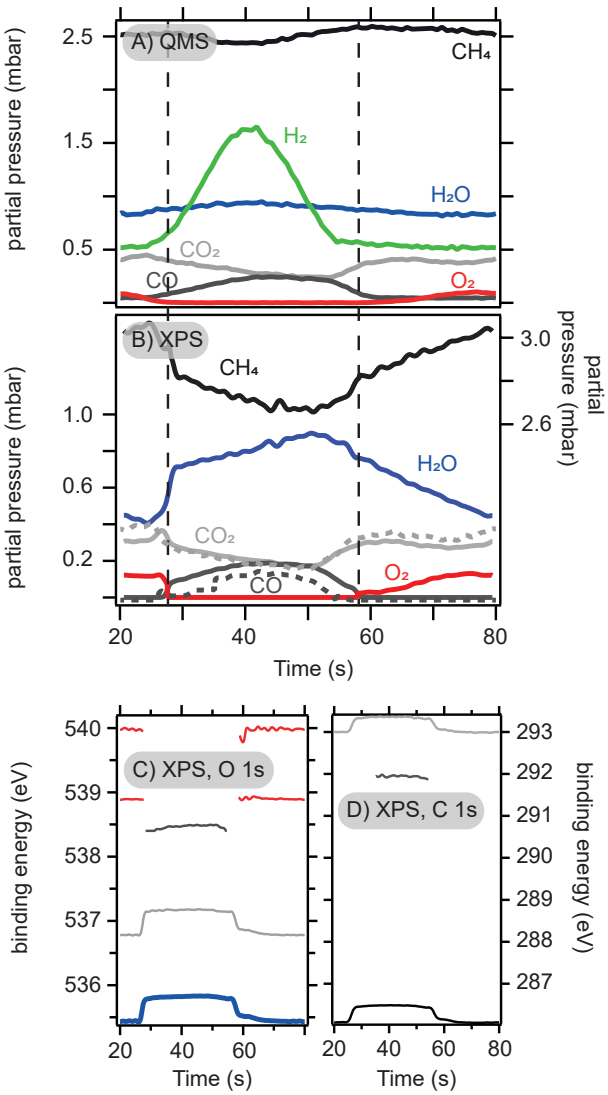

Figure S5: (A) Partial pressures of mass spectrometer data together with all those calculated from the curve fit to the APXPS gas phase spectra (B). The vertical dashed lines indicate the beginning and end of the O-MTL. The corresponding apparent binding energies of the O 1s and C 1s components are shown in (C,D).

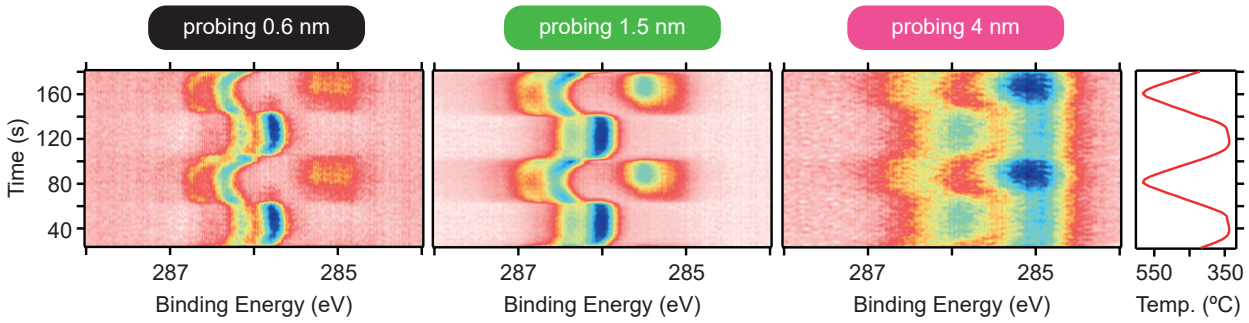

Figure S6: C 1s spectra measured under similar conditions, just with a slightly larger temperature amplitude, i.e. 340 °C (50 s) to 584 °C (30 s). Carbon is fully removed from the surface but never from the bulk.

References

(1) Campbell, J. L.; Papp, T. Widths of the atomic K-N7 levels. *Atomic Data and Nuclear Data Tables* **2001**, *77*, 1–56.

(2) Knudsen, J.; Eads, C.; Klyushin, A.; Temperton, R.; Küst, U.; Boix, V.; Kraina, A.; Scardamaglia, M.; Shavorskiy, A.; Kokkonen, E.; Schnadt, J. Catalysis in frequency space: Resolving hidden surface structure and activity oscillations. *to be accepted in ACS Catalysis* **2024**, preprint: 10.21203/rs.3.rs-4242040/v1.

(3) Küst, U.; Prumbs, J.; Eads, C.; Wang, W.; Boix, V.; Klyushin, A.; Scardamaglia, M.; Temperton, R.; Shavorskiy, A.; Knudsen, J. Comparing phase sensitive detection and Fourier analysis of modulation excitation spectroscopy data exemplified by Ambient Pressure X-ray Photoelectron Spectroscopy. *Surface Science* **2025**, *751*, 122612.

(4) Knudsen, J.; Gallo, T.; Boix, V.; Strømsheim, M.; Acunto, G. D. .; Goodwin, C.; Wallander, H.; Zhu, S.; Soldemo, M.; Cavalca, F.; Scardamaglia, M.; Degerman, D.; Nilsson, A.; Amann, P.; Shavorskiy, A. Stroboscopic operando spectroscopy of the dynamics in heterogeneous catalysis by event-averaging. *Nature Communications* **2021**,